

LHCEWWG

Di-Boson Group Report

1 **Fiducial cross section and triple gauge coupling definitions for di-boson**
2 **measurements**

3 ATLAS, CMS

4 **Abstract**

5 This note presents a summary of preliminary fiducial cross section definitions and anoma-
6 lous triple gauge coupling parametrisations planned to be used in di-boson measurement
7 with ATLAS and CMS on the full 2012 data set.

8	Contents	
9	1 Introduction	2
10	2 ZZ analyses	3
11	2.1 ATLAS 7 TeV ZZ Analysis	3
12	2.1.1 Event Selection: $ZZ \rightarrow \ell^+ \ell^- \ell'^+ \ell'^-$	3
13	2.1.2 Event Selection: $ZZ \rightarrow \ell^+ \ell^- \nu \bar{\nu}$	4
14	2.1.3 Background Estimation	4
15	2.1.4 Uncertainties	5
16	2.2 CMS 7 TeV ZZ Analysis	5
17	2.2.1 Event Selection	5
18	2.2.2 Background Estimation	8
19	2.2.3 Uncertainties	8
20	3 ZZ combination	11
21	3.1 Theoretical framework for anomalous couplings	11
22	3.2 Anomalous coupling signal modeling (Re-weighting Procedure)	12
23	3.3 Statistical method used for the combination	12
24	3.4 Treatment of systematic uncertainties	14
25	3.5 Combination Results	16
26	3.6 Comment on unitarization issues	16
27	4 Conclusions	19

28 **1 Introduction**

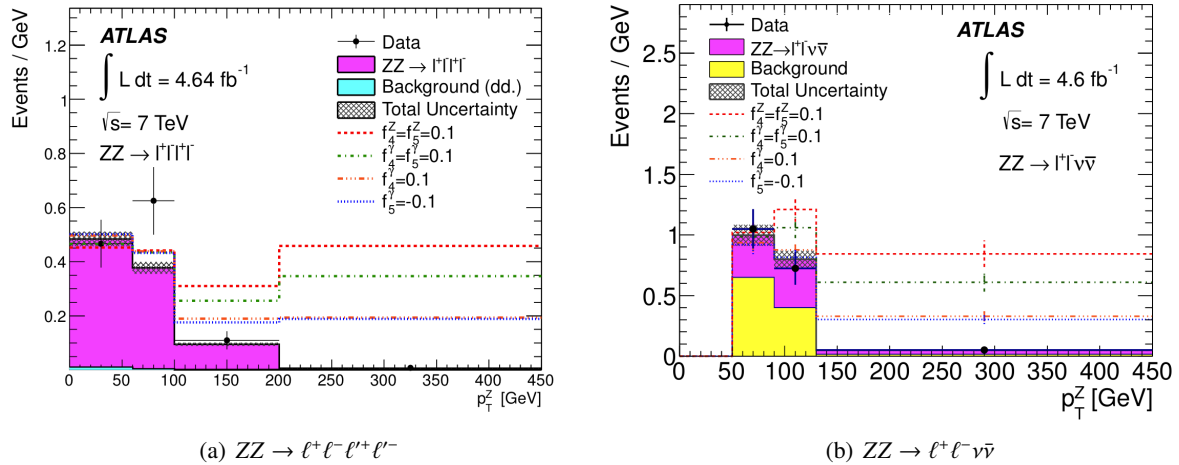


Figure 1: The transverse momentum distribution of the Z boson with the highest transverse momentum. The predicted distributions for four different aTGC values at $\Lambda = 3$ TeV are shown as dashed lines [1].

2 ZZ analyses

2.1 ATLAS 7 TeV ZZ Analysis

The ATLAS analysis of ZZ production uses two decay channels, $ZZ \rightarrow \ell^+ \ell^- \nu \bar{\nu}$ and $ZZ \rightarrow \ell^+ \ell^- \ell'^+ \ell'^-$. As in the $W^\pm Z$ analysis, ℓ refers to an electron or a muon. The $ZZ \rightarrow \ell^+ \ell^- \ell'^+ \ell'^-$ selection is broken into two categories, ZZ and ZZ* where the Z* boson is off shell. This section is summarizing the selection details, background estimation, and uncertainties from Reference [1] used to extract the anomalous triple gauge coupling intervals. Plots of the reconstructed Z p_T distributions used to extract the aTGC intervals are shown in Figure 1.

2.1.1 Event Selection: $ZZ \rightarrow \ell^+ \ell^- \ell'^+ \ell'^-$

The event is required to have exactly four leptons and fired at least a single electron or single muon event trigger. All pairs of leptons in the event must be separated by $\Delta R > 0.2$. Out of the four leptons, at least one muon must have $p_T > 20$ GeV or at least one electron must have $p_T > 25$ GeV and be matched to the online electron or muon that triggered the event to ensure a high trigger efficiency. The remaining leptons have a $p_T > 7$ GeV requirement. All the leptons must pass an isolation requirement where the calorimeter and track isolation measurements within a ΔR cone of 0.2 must be less than 30% and 15% of the lepton p_T respectively. Generally, electrons must have a pseudorapidity of $|\eta| < 2.47$ and muons must have $0.1 < |\eta| < 2.5$.

The overall selection is extended by looking for electrons and/or muons from an extended $|\eta|$ range. These muons come in two categories, calorimeter tagged muons from a region with poor muon spectrometer coverage, $|\eta| < 0.1$, and forward spectrometer muons, $2.5 < |\eta| < 2.7$. These muons must have $p_T > 10$ GeV and a calorimeter isolation within a $\Delta R < 0.2$ cone that is less than 15% of the muon p_T . Calorimeter tagged muons are built with calorimeter clusters and are matched to inner detector tracks with $p_T > 20$ GeV. Only one muon from each of these categories is allowed and it must be paired with a non-extended muon in forming a Z boson.

The extended electrons come from the range $2.5 < |\eta| < 3.16$ and are required to have $p_T > 20$ GeV. As this is outside the inner detector fiducial coverage region, no track or charge information is available for these electrons. Electron identification comes entirely from the longitudinal and transverse shower

56 profile in the calorimeter. No isolation requirement is imposed. Only one is allowed in an event and it is
57 assigned the opposite charge as the same flavor lepton it is paired with.

58 Same flavor, oppositely charged lepton pairs are used to reconstruct Z boson candidates. Two Z boson
59 candidates are required for each event. In the channels with four same flavor leptons, the pairs are
60 selected to minimize the difference between the pair's invariant mass and the global average mass of the
61 Z boson. For the aTGC measurement, both Z boson candidates must have an invariant mass between 66
62 and 116 GeV.

63 With these selections, 66 $ZZ \rightarrow \ell^+ \ell^- \ell'^+ \ell'^-$ candidate events are observed in data. Seven of these
64 candidates contain extended $|\eta|$ range leptons.

65 2.1.2 Event Selection: $ZZ \rightarrow \ell^+ \ell^- \nu \bar{\nu}$

66 The leptons in these events are required to have $p_T > 20$ GeV and have the same trigger matching
67 requirements as the $ZZ \rightarrow \ell^+ \ell^- \ell'^+ \ell'^-$ selection. The isolation requirements are changed as the isolation
68 cone size is increased to $\Delta R < 0.3$. Both track and calorimeter isolation measurements are required to be
69 less than 15% of the lepton p_T . Each event must have exactly two same flavor, oppositely charged leptons
70 with an invariant mass between 76 and 106 GeV. The lepton pair must also be separated by $\Delta R > 0.3$
71 reflecting the larger isolation cone used.

72 Jets are used as a veto for background events in the $ZZ \rightarrow \ell^+ \ell^- \nu \bar{\nu}$ channel. The jets are reconstructed
73 with the anti- k_t algorithm [2] with a radius of $R = 0.4$. The veto jets are required to have $p_T > 25$ GeV
74 and $|\eta| < 4.5$. A requirement that the scalar sum of the track p_T associated with the jet and originating
75 from the primary vertex be at least 75% of the total scalar sum of the p_T of all the tracks associated
76 with the jet is used to reduce the impact of pile up jets. Any jets that lie within $\Delta R < 0.3$ of a lepton is
77 discarded. If any veto jets are found, the event is rejected. The event is also rejected if there are any jets
78 with $p_T > 20$ GeV that did not result from the proton-proton collision.

79 The last requirement for these events is to have a large missing transverse energy, indicative of the
80 second Z boson decaying to neutrinos. The ZZ boson pair are expected to be produced back to back,
81 the E_T^{miss} is modified into something called axial- E_T^{miss} to further eliminate backgrounds. Axial- E_T^{miss} is
82 defined as $-E_T^{\text{miss}} \cdot \vec{p}^Z / p_T^Z$. The axial- E_T^{miss} must be greater than 75 GeV. A final distinguishing variable
83 is the fractional p_T difference, $|E_T^{\text{miss}} - p_T^Z| / p_T^Z$. The fractional p_T difference must be less than 0.4.
84 $W^\pm Z$ events making it through the selection are reduced by rejecting any events with a third lepton with
85 $p_T > 10$ GeV. After all these selections, 87 $ZZ \rightarrow \ell^+ \ell^- \nu \bar{\nu}$ candidates are observed in data.

86 2.1.3 Background Estimation

87 The background estimate for $ZZ \rightarrow \ell^+ \ell^- \ell'^+ \ell'^-$ was performed using data driven techniques similar to
88 those described in Section ?? in the $W^\pm Z$ analysis. A fake factor, f , is calculated using cut regions with
89 one Z boson plus real and fake leptons. f used to estimate the number of background events that make
90 it into the signal selection region by extrapolating from two regions dominated by background, those
91 with three selected leptons and a fourth failing select cuts and those with two selected leptons with two
92 additional leptons failing select cuts. See Reference [1] for exact details. Table 1 contains the number of
93 events observed, the expected signal and the expected background in each Z p_T bin.

94 The $ZZ \rightarrow \ell^+ \ell^- \nu \bar{\nu}$ has far more processes contributing to its background and a much wider variety of
95 techniques were used to estimate it. The background contribution from $t\bar{t}$, Wt , W^+W^- and $Z \rightarrow \tau^+\tau^-$ was
96 calculated with a data driven method that looked for events with one electron and one muon passing the
97 lepton selection. These background events were then extrapolated into the signal region using the ratio
98 of the efficiencies of ee and $\mu\mu$ to the efficiency of $e\mu$. Backgrounds from $W^\pm Z$ events where one lepton
99 is lost were estimated with simulated $W^\pm Z$ events. Backgrounds from the Z +jets process used a data
100 driven template method (see [1]). Finally, the background from events with a misidentified lepton were

Source	$0 < p_T^Z < 60$ GeV	$60 < p_T^Z < 100$ GeV	$100 < p_T^Z < 200$ GeV	$p_T^Z > 200$ GeV
Data	28	25	11	2
ZZ SM Signal	27.9	14.6	9.3	1.6
Background	0.6	0.2	0.1	0.1

Table 1: Observed and predicted events entering into aTGC extraction in the $ZZ \rightarrow \ell^+ \ell^- \ell'^+ \ell'^-$ channel.

Source	$50 < p_T^Z < 90$ GeV	$90 < p_T^Z < 130$ GeV	$p_T^Z > 130$ GeV
Data	42	29	16
ZZ SM Signal	13.6	15.7	10.1
MC Backgrounds	8.5	8.4	4.1
Data Driven Backgrounds	17.5	7.6	0.8

Table 2: Observed and predicted events entering into aTGC extraction in the $ZZ \rightarrow \ell^+ \ell^- \bar{\nu} \nu$ channel.

101 extracted from data using the matrix method [1], [3]. Table 2 contains the number of events observed,
 102 the expected signal and the expected background in each Z p_T bin.

103 2.1.4 Uncertainties

104 All the uncertainties used in the aTGC interval extraction are listed in Tables 3 and 4. The luminosity
 105 uncertainty was 3.9% in all bins and all channels. The ‘‘Systematics’’ uncertainty listed in the tables
 106 comes from the combination of lepton efficiency, lepton energy/momentum, lepton isolation and impact
 107 parameter, jet and E_T^{miss} modeling, the jet veto, and trigger efficiencies. These uncertainties affect the
 108 signal estimation and any background estimations made with MC. The ZZ theory uncertainty comes
 109 from the combination of PDF, renormalization and factorization scale uncertainties. The data driven
 110 systematic uncertainty for the $ZZ \rightarrow \ell^+ \ell^- \ell'^+ \ell'^-$ background comes from the combined uncertainty on
 111 the calculated fake factor, f . The systematics on the data driven background for the $ZZ \rightarrow \ell^+ \ell^- \bar{\nu} \nu$
 112 channel come from systematics on MC backgrounds used in the calculations and from uncertainties
 113 on extrapolation factors. With the exception of the statistical uncertainties, all the uncertainties were
 114 considered correlated across the Z p_T bins and the 4ℓ and $2\ell 2\nu$ decay channels.

115 2.2 CMS 7 TeV ZZ Analysis

116 The CMS analysis of the ZZ aTGCs at $\sqrt{s} = 7$ TeV used 5.0 fb^{-1} of recorded data. The data was searched
 117 for events with two same flavor opposite charge pairs of leptons (muons or electrons) that could be the
 118 decay products of a ZZ boson pair. This section will summarize the event selection, backgrounds, and
 119 systematics used in the CMS 7 TeV ZZ analysis found in Reference [4].

120 2.2.1 Event Selection

121 Events were selected by searching for pairs of oppositely charged electrons or muons. Electron candi-
 122 dates had to fall within $|\eta| < 2.5$ with $p_T > 7$ GeV and muons had to fall within $|\eta| < 2.4$ with $p_T > 5$
 123 GeV. One of the leptons was required to have $p_T > 20$ GeV and the second had to have $p_T > 10$ GeV.
 124 The invariant mass of the lepton pair was required to fall within $60 < m_{\ell\ell} < 120$ GeV. Both of these
 125 leptons had an isolation requirement where the pile corrected total energy in tracks, the EM calorimeter,
 126 and the hadronic calorimeter within a $\Delta R < 0.3$ cone be less than 27.5% of the magnitude of the trans-
 127 verse momentum of the lepton. The lepton pair meeting these requirements with invariant mass closest
 128 Z boson mass was selected as Z_1 while second Z boson was labeled as Z_2 .

Uncertainty	$0 < p_T^Z < 60$ GeV	$60 < p_T^Z < 100$ GeV	$100 < p_T^Z < 200$ GeV	$p_T^Z > 200$ GeV
ZZ statistics	0.9%	1.2%	1.5%	3.9%
Luminosity	3.9%	3.9%	3.9%	3.9%
Systematics	3.5%	3.8%	4.0%	4.5%
ZZ Theory	6.4%	7.1%	8.5%	16.1%
Data Driven Background Systematics	76.2%	75.0%	77.8%	72.7%
Data Driven Background Statistics	119.0%	120.0%	111.1%	90.9%

Table 3: ATLAS uncertainties on signal and background in the $ZZ \rightarrow \ell^+ \ell^- \ell'^+ \ell'^-$ channel used in the aTGC interval extraction. The first three uncertainties apply to the ZZ prediction, the final two apply to the data driven backgrounds.

Uncertainty	$50 < p_T^Z < 90 \text{ GeV}$	$90 < p_T^Z < 130 \text{ GeV}$	$p_T^Z > 130 \text{ GeV}$
ZZ statistics	1.6%	1.8%	1.4%
Luminosity	3.9%	3.9%	3.9%
Systematics	2.0%	3.1%	3.9%
ZZ Theory	9.5%	10.5%	13.3%
Data Driven Background Systematics	6.4%	9.0%	24.4%
Data Driven Background Statistics	25.1%	35.5%	217.9%
MC Background Systematics	2.2%	2.3%	2.2%
MC Background Statistics	9.1%	8.8%	15.9%

Table 4: ATLAS uncertainties on signal and background in the $ZZ \rightarrow \ell^+ \ell^- \bar{\nu} \nu$ channel used in the aTGC interval extraction. The first three uncertainties apply to the ZZ prediction, the final two apply to the data driven backgrounds.

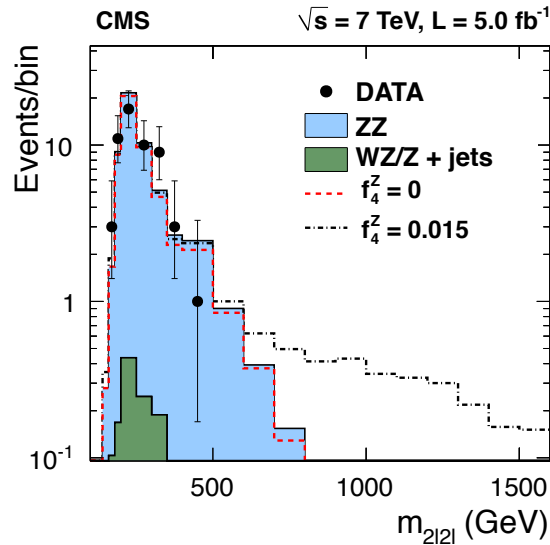


Figure 2: The distribution of the four lepton invariant mass for the sum of the $eeee$, $e\mu\mu$, and the $\mu\mu\mu\mu$ channels [4].

129 2.2.2 Background Estimation

130 As with the ATLAS analysis, the CMS analysis estimated its background using a data driven technique.
 131 The rate for non-isolated leptons that are misidentified as isolated leptons was measured using a control
 132 region with no ZZ signal contribution. Events that contained the selected Z_1 boson and only a single
 133 probe electron or muon that has no isolation requirement were used. The misidentification rate was
 134 then calculated as the ratio of the number of probes that pass the isolation to the total number of probe
 135 candidates. This rate was measure as a function of p_T and η for muons and electrons respectively. The
 136 background estimation in the signal region was then estimated by measuring the number of events in a
 137 third control region that had all the Z_1 and Z_2 selection requirements except the isolation requirements
 138 were reversed. Table 5 contains the observed events, the estimated SM signal, and the estimated back-
 139 ground events in bins of m_{ZZ} used in the aTGC extraction.

140 2.2.3 Uncertainties

141 The uncertainties used in the CMS aTGC extraction are outlined in Table 6. The same relative uncertainty
 142 value was used in each m_{ZZ} bin. The data driven background uncertainty was treated as correlated
 143 across the m_{ZZ} bins but uncorrelated across the three decay channels: $4e$, 4μ , and $2e2\mu$. The data driven
 144 background uncertainty was measured on the values of the misidentification rates and the limited quantity
 145 of data in the control regions. The uncertainty on ZZ includes the PDF uncertainty, renormalization and
 146 factorization scales uncertainty, reconstruction uncertainty, uncertainty on aTGC signal reweighting and
 147 statistical uncertainty.

m_{ZZ} bin	(100, 200) GeV	(200, 300) GeV	(300, 400) GeV	(400, 600) GeV	(600, 800) GeV
	$ZZ \rightarrow \mu^+ \mu^- \mu^+ \mu^-$				
Data	4	8	1	1	0
ZZ SM Signal	2.8	8.7	2.1	0.8	0.2
Background	0.2	0.4	0.1	0.0	0.0
	$ZZ \rightarrow e^+ e^- \mu^+ \mu^-$				
Data	8	15	8	0	0
ZZ SM Signal	5.0	14.1	3.2	1.4	0.3
Background	0.2	0.3	0.2	0.0	0.0
	$ZZ \rightarrow e^+ e^- e^+ e^-$				
Data	2	4	3	0	0
ZZ SM Signal	2.0	5.5	1.2	0.5	0.1
Background	0.1	0.1	0.1	0.0	0.0

Table 5: CMS observed and predicted events entering into aTGC extraction.

Source	(%)
ZZ Signal modeling (reweighintg, statistics, reconstruction)	13.4
ZZ Theory (PDF, scale)	4.0
Data Driven Background	30.0
Luminosity	2.2

Table 6: CMS uncertainties used in the aTGC extraction.

148 3 ZZ combination

149 The combination of anomalous coupling results by ATLAS and CMS collaboration was performed using
150 published results for ZZ production channels with full 7 TeV dataset.

151 A likelihood is used to extract the 95% confidence interval with using Bayesian integration and Ney-
152 man construction techniques.

153 Systematic uncertainties are included as nuisance parameters, correlations and bin-to-bin migrations
154 are taken into account.

155 There are many differences between ATLAS and CMS anomalous coupling measurements. First,
156 different observables were used. Anomalous couplings results with increase of a cross section at high
157 energies, therefore diboson system mass and boson transverse momentum are particularly sensitive. AT-
158 LAS is using leading Z transverse momentum while CMS uses diboson system mass. Theoretical uncer-
159 tainties on the signal are p_T dependent but flat in diboson mass, this results with signal shape dependent
160 uncertainty used by ATLAS and flat uncertainty used by CMS.

161 Anomalous coupling signal model continuous in anomalous coupling parameters was built differently
162 in two experiments as described in section 3.2.

163 Several differences were also found in the statistical methods for limit setting. These are described
164 in detail in section 3.3.

165 3.1 Theoretical framework for anomalous couplings

166 Neutral trilinear gauge couplings are forbidden at the tree level, but allowed in some extensions of the
167 SM . The ZZ production enables to probe the existence of anomalous couplings in the ZZZ and γZZ
168 vertices.

169 Neutral couplings $V^{(*)}ZZ$ ($V = Z, \gamma$) can be described using the effective Lagrangian [5]:

$$170 \quad \mathcal{L}_{VZZ} = -\frac{e}{M_Z^2} \left\{ \left[f_4^\gamma (\partial_\mu F^{\mu\alpha}) + f_4^Z (\partial_\mu Z^{\mu\alpha}) \right] Z_\beta (\partial^\beta Z_\alpha) - \left[f_5^\gamma (\partial^\mu F_{\mu\alpha}) + f_5^Z (\partial^\mu Z_{\mu\alpha}) \right] \tilde{Z}^{\alpha\beta} Z_\beta \right\}, \quad (1)$$

171 where Z represents the Z boson and $F_{\mu\alpha}$ represents the electromagnetic field tensor. The coefficients
172 f_i^γ and f_i^Z correspond to couplings $\gamma^{(*)}ZZ$ and $Z^{(*)}ZZ$ where the terms corresponding to f_4^V parameters
173 violate the CP symmetry, and the terms corresponding to f_5^V parameters conserve CP.

174 ATLAS analysis includes anomalous coupling measurement with two form factor scales, $\Lambda_{FF} = 2$
175 TeV and $\Lambda_{FF} = \infty$, while CMS analysis uses the approach without form factor equivalent to $\Lambda_{FF} = \infty$.
176 Therefore combined limit was derived for approach without form factor.

177 3.2 Anomalous coupling signal modeling (Re-weighting Procedure)

178 Simulated events generated with *SHERPA* [6] generator were used by both ATLAS and CMS to model
179 anomalous coupling signal.

180 In CMS analysis events were generated and simulated with several non Standard Model values of
181 anomalous neutral $ZZ\gamma$ coupling. Two anomalous coupling parameters were varied at the same time,
182 (f_4^γ, f_4^Z) and (f_5^γ, f_5^Z) , while other parameters were set to Standard Model value. Signal model continuous
183 in anomalous coupling parameters was achieved by performing two dimensional second order polyno-
184 mial fit on simulated expected yield in every observable bin.

185 In ATLAS analysis reweighting of Sherpa events was performed using the BaurRainwater [7, 8] and
186 BHO [9] MC generators. The re-weighting procedure allows to re-weight a sample of event simulated
187 with a given set of coupling parameters to another arbitrary set of couplings parameters. It is possible to
188 generate ZZ events with any anomalous TGC $(f_4^\gamma, f_4^Z, f_5^\gamma)$ with . Each event has a vector of 15 weights
189 $\{w_0 \dots w_{14}\}$ which can be reweighted to another anomalous TGC phase space point. The weight at a new
190 point is given by

$$\begin{aligned} w(f_4^\gamma, f_4^Z, f_5^\gamma, f_5^Z) &= w_0 + (f_4^\gamma)^2 w_1 + (f_4^Z)^2 w_2 + (f_5^\gamma)^2 w_3 + (f_5^Z)^2 w_4 \\ &+ 2f_4^\gamma w_5 + 2f_4^Z w_6 + 2f_5^\gamma w_7 + 2f_5^Z w_8 \\ &+ 2f_4^\gamma f_4^Z w_9 + 2f_4^\gamma f_5^\gamma w_{10} + 2f_4^\gamma f_5^Z w_{11} + 2f_4^Z f_5^\gamma w_{12} + 2f_4^Z f_5^Z w_{13} + 2f_5^\gamma f_5^Z w_{14} \end{aligned} \quad (2)$$

191 To re-weight to another value of the form factor Λ_{FF} , the anomalous TGC parameters $\alpha = (f_4^\gamma, f_4^Z,$
192 $f_5^\gamma, f_5^Z)$ are multiplied by $\zeta = (1 + \frac{\hat{s}}{\Lambda_{FF}^2})^3 (1 + \frac{\hat{s}}{\Lambda'_{FF}{}^2})^{-3}$, where Λ_{FF} is the cutoff used in generating the
193 original sample, and Λ'_{FF} is the target value. This is equivalent to adjusting the event weights $\{w_0 \dots w_{14}\}$
194 as

$$w_i \rightarrow \begin{cases} w_i & \text{for } i = 0 \\ w_i \zeta & \text{for } i = 5, 6, 7, 8 \\ w_i \zeta^2 & \text{for } i = 1, 2, 3, 4, 9, 10, 11, 12, 13, 14 \end{cases} \quad (3)$$

195 After applying these factors, the event weights are accumulated for the MC signal events that pass
196 the selection and correct with additional scale factors related to reconstruction, trigger and pile-up de-
197 scription. The end result is the expected number of signal events N_s^i in our data sample in the form
198 of

$$\begin{aligned} N_s^i(\alpha) &= W_0^i + (f_4^\gamma)^2 W_1 + (f_4^Z)^2 W_2 + (f_5^\gamma)^2 W_3 + (f_5^Z)^2 W_4 \\ &+ 2f_4^\gamma W_5 + 2f_4^Z W_6 + 2f_5^\gamma W_7 + 2f_5^Z W_8 \\ &+ 2f_4^\gamma f_4^Z W_9 + 2f_4^\gamma f_5^\gamma W_{10} + 2f_4^\gamma f_5^Z W_{11} + 2f_4^Z f_5^\gamma W_{12} + 2f_4^Z f_5^Z W_{13} + 2f_5^\gamma f_5^Z W_{14} \end{aligned} \quad (4)$$

199 for each bin in a histogram.

200 Both approaches of signal description in anomalous coupling parameter space are consistent, making
201 the translation between them trivial. Sets of two parameters were varied simultaneously providing a two
202 dimensional model in parameter space by both experiments. Coefficients $\{W_j^i\}$ are used in the anomalous
203 TGC limit setting procedure described in section 3.3.

204 3.3 Statistical method used for the combination

205 To set limits on the anomalous TGC paramters, two different limit approaches were used, frequentist
206 and delta log-likelihood method. The reweighting procedure described in the previous section allows
207 us to express expected number of signal events N_{sig}^i in observable bin as a function of anomalous TGC
208 parameters.

209 The likelihood is built from a series of components. First is the model prediction of the number of
210 events in each bin and these are defined as

$$N_{\text{sig}}^i(\boldsymbol{\alpha}, \boldsymbol{\theta}) = N_{\text{sig}}^i(\boldsymbol{\alpha}) \prod_j^J (1 + \delta^{ij})^{\theta^j} \quad (5)$$

$$N_{\text{bkg}}^i(\boldsymbol{\theta}) = N_{\text{bkg}}^i \prod_j^J (1 + \delta^{ij})^{\theta^j} \quad (6)$$

211 resulting with the nuisance effect following log-normal distribution. Here, N_{bkg}^i is the background
212 prediction in bin i , δ^{ij} is the value of the j^{th} uncertainty in bin i , and θ^j is the nuisance parameter
213 associated with the j^{th} uncertainty. Another approach would be to use Gaussian distribution as done in
214 the ATLAS measurement:

$$N_{\text{sig}}^i(\boldsymbol{\alpha}, \boldsymbol{\theta}) = N_{\text{sig}}^i(\boldsymbol{\alpha}) \prod_j^J (1 + \theta^j \delta^{ij}) \quad (7)$$

$$N_{\text{bkg}}^i(\boldsymbol{\theta}) = N_{\text{bkg}}^i \prod_j^J (1 + \theta^j \delta^{ij}) \quad (8)$$

215 where also a different approach for total effect from all uncertainties was used:

$$N_{\text{sig}}^i(\boldsymbol{\alpha}, \boldsymbol{\theta}) = N_{\text{sig}}^i(\boldsymbol{\alpha}) \left(1 + \sum_j^J \theta^j \delta^{ij}\right) \quad (9)$$

$$N_{\text{bkg}}^i(\boldsymbol{\theta}) = N_{\text{bkg}}^i \left(1 + \sum_j^J \theta^j \delta^{ij}\right) \quad (10)$$

216 For a short hand, define $\psi^i(\boldsymbol{\alpha}, \boldsymbol{\theta}) = N_{\text{sig}}^i(\boldsymbol{\alpha}, \boldsymbol{\theta}) + N_{\text{bkg}}^i(\boldsymbol{\theta})$. The likelihood of observing N_{data}^i events
217 given $\psi^i(\boldsymbol{\alpha}, \boldsymbol{\theta})$ is then described by a Poisson distribution. The likelihood is completed multiplying the
218 Poisson distribution by the constraint on the nuisance parameters.

$$L(\boldsymbol{\alpha}, \boldsymbol{\theta}) = \prod_{i=1}^I \frac{[\psi^i(\boldsymbol{\alpha}, \boldsymbol{\theta})]^{N_{\text{data}}^i} e^{-\psi^i(\boldsymbol{\alpha}, \boldsymbol{\theta})}}{N_{\text{data}}^i!} \times \frac{1}{(2\pi)^J} e^{-\frac{1}{2}\boldsymbol{\theta}^2}, \quad (11)$$

219 The most likely estimators (MLE) for the aTGCs and nuisance parameters are then found by finding
220 the minimum of the negative log of Equation 11. Finding the 95% confidence interval in the Frequentist
221 sense now means a comparison must be made to many other “experiments”. Since the experiment cannot
222 be repeated many times, pseudo-experiments are used. These pseudo experiments are just a count of
223 events that are generated for each bin i . The count of events are generated by randomly sampling a
224 Poisson distribution with a mean of $\psi^i(\boldsymbol{\alpha}_{\text{test}}, \hat{\boldsymbol{\theta}})$. Parametric bootstrap scheme was used where $\hat{\boldsymbol{\theta}}$ are the
225 nuisance parameter values that maximize the likelihood acting on N_{data} when $\boldsymbol{\alpha}$ is held fixed at $\boldsymbol{\alpha}_{\text{test}}$. The
226 likelihood for the pseudo-experiment is modified to the following form

$$L(\boldsymbol{\alpha}, \boldsymbol{\theta}) = \prod_{i=1}^I \frac{[\psi^i(\boldsymbol{\alpha}, \boldsymbol{\theta})]^{N_{\text{pseudo}}^i} e^{-\psi^i(\boldsymbol{\alpha}, \boldsymbol{\theta})}}{N_{\text{pseudo}}^i!} \times \frac{1}{(2\pi)^J} e^{-\frac{1}{2}(\boldsymbol{\theta} - \boldsymbol{\theta}_0)^2} \quad (12)$$

227 The θ_0 represents a small random Gaussian shift in the central values of the nuisance parameters
 228 that is added for each pseudo-experiment to represent how a different experiment would have different
 229 estimates for its uncertainties. Ten thousand pseudo-experiments are generated to determine the p-value
 230 at a test point, α_{test} . The p-value at a test point is defined as

$$\text{p-value}(\alpha_{\text{test}}) = \frac{\text{Number of pseudo experiments with less likely results than observed}}{\text{Total number of pseudo experiments}} \quad (13)$$

231 Evaluating the numerator in Equation 13 requires a way to compare how likely a pseudo-experiment
 232 is to N_{data} . This is accomplished through the use of the profile likelihood ratio, $\lambda(\alpha)$.

$$\lambda(\alpha_{\text{test}}) = \frac{L(\alpha_{\text{test}}, \hat{\theta})}{L(\hat{\alpha}, \hat{\theta})} \quad (14)$$

233 α_{test} is the aTGC point being tested, $\hat{\theta}$ are the nuisance parameter values that maximize the likelihood
 234 at α_{test} , and $\hat{\alpha}$ and $\hat{\theta}$ are the values of α and θ that maximize the likelihood together. As a result,
 235 $0 < \lambda(\alpha) < 1$. Pseudo-experiments with $\lambda(\alpha)$ that is less than the $\lambda(\alpha)$ found on data are considered less
 236 likely. Points are tested moving out from $\hat{\alpha}$ in the positive and negative directions until the upper and
 237 lower points are found with p-value equal to 5%. These points bound the 95% confidence interval.

238 The limit setting criteria described above is called the Feldman-Cousins method [10].

239 A much faster method for extracting the intervals involves defining a test statistic that uses the profile
 240 likelihood ratio.

$$t_\alpha = -2 \ln \lambda(\alpha) \quad (15)$$

241 In this case, t_α is assumed to follow a χ^2 distribution so the probability is read directly as a result
 242 of this value. The test points where $t_\alpha = 3.84$ bound the 95% confidence interval when only a single
 243 aTGC value is allowed to float. This method for extracting the 95% confidence interval is commonly
 244 referred to as the delta log-likelihood method as another way to write the test statistic is as $t_\alpha/2 =$
 245 $\ln[L(\hat{\alpha}, \hat{\theta})] - \ln[L(\alpha_{\text{test}}, \hat{\theta})]$

246 Expected intervals are also calculated for the combined ATLAS and CMS inputs. All intervals pre-
 247 sented were calculated using an pre-fit Asimov dataset. An Asimov dataset is a special kind of pseudo-
 248 experiment used for quickly extracting expected limits. Nominally and also used in ATLAS measurement
 249 paper, extracting expected limits involves running many pseudo-experiments in the same manner as used
 250 to build the p-value distribution discussed earlier in this section but only at the standard model expecta-
 251 tion (background only). Each of these pseudo-experiments then has its interval calculated with one or
 252 both of the methods described earlier. The average of the upper and lower intervals for all the pseudo-
 253 experiments is then taken as the expected interval. An Asimov dataset takes the most average version of
 254 the pseudo-experiments, $\psi^i(\mathbf{0}, \tilde{\theta})$, where $\tilde{\theta}$ is the nominal value of nuisances, and extracts a single interval
 255 with it. As this pseudo-experiment is the average, the 95% confidence interval should converge to the
 256 values found on the average interval as the number of pseudo-experiments tested approaches infinity.

257 In ATLAS measurement the Feldman-Cousins method was used to set the limits on anomalous cou-
 258 plings, while in CMS measurement the modified frequentist construction CL_S method [11, 12, 13] was
 259 used.

260 3.4 Treatment of systematic uncertainties

261 For the combination of ATLAS and CMS data only luminosity, PDF and QCD scale uncertainty on signal
 262 are treated as 100% correlated. Other uncertainties are statistical or detector related and these are treated
 263 as uncorrelated.

Source	Affected processes	Uncertainty value (ATLAS/CMS)
Luminosity	ZZ signal, MC driven background	3.9% / 2.2%
PDFs+ α_S	ZZ signal	6.4%-16.1% (shape) / 4%

Table 7: Table of 100% correlated uncertainties

Source	Affected processes	Uncertainty (ATLAS/CMS)
MC statistics	ZZ signal, MC driven background	shape, uncorrelated bins
data-driven method statistics	data driven background	shape / flat
data-driven method systematics	data driven background	shape / flat
MC systematics	MC driven background	shape / -
Reconstruction	ZZ signal, MC driven background	shape / flat

Table 8: Table of 100% uncorrelated uncertainties

264 Luminosity uncertainty is correlated since it is driven by machine-dependent uncertainties.

265 Theoretical uncertainties on signal, due to QCD scales and PDFs, are calculated separately in ATLAS
 266 and CMS. Since the source of uncertainties is the same the uncertainties are 100% correlated between
 267 CMS and ATLAS.

268 Expected background contribution in both analysis is mainly (or completely) derived from the data.
 269 The methods are not identical and reconstructions in detectors are different therefore the uncertainties on
 270 the estimated backgrounds are used as uncorrelated.

271 Full list of uncertainties can be found in Tables 7 and 8.

272 **3.5 Combination Results**

Expected deltaNLL limit	f_4^Y		f_4^Z	
	ATLAS	CMS	ATLAS	CMS
Gaussian	[-0.0121, 0.0125]	[0.0120, 0.0125]	[-0.0103, 0.0105]	[-0.0103, 0.0105]
log-Normal	[-0.0120, 0.0123]	[0.0119, 0.0123]	[-0.0102, 0.0104]	[-0.0102, 0.0104]
Observed deltaNLL limit	f_5^Y		f_5^Z	
	ATLAS	CMS	ATLAS	CMS
Gaussian	[-0.0127, 0.0121]	[0.0126, 0.0121]	[-0.0106, 0.0104]	[0.0106, 0.0104]
log-Normal	[-0.0126, 0.0119]	[0.0125, 0.0120]	[-0.0105, 0.0103]	[0.0105, 0.0103]
Observed deltaNLL limit	f_4^Y		f_4^Z	
	ATLAS	CMS	ATLAS	CMS
Gaussian	[-0.0103, 0.0108]	[0.0103, 0.0109]	[-0.00875, 0.00912]	[0.00874, 0.00913]
log-Normal	[-0.0102, 0.0108]	[0.0102, 0.0108]	[-0.00870, 0.00907]	[0.00871, 0.00909]
Observed deltaNLL limit	f_5^Y		f_5^Z	
	ATLAS	CMS	ATLAS	CMS
Gaussian	[-0.0108, 0.0103]	[0.0108, 0.0104]	[-0.00907, 0.00891]	[0.00909, 0.00891]
log-Normal	[-0.0108, 0.0103]	[0.0108, 0.0103]	[-0.00902, 0.00885]	[0.00906, 0.00886]

Table 9: Table of expected and observed intervals for the combined ATLAS and CMS inputs. Intervals were all extracted with the delta log-likelihood method.

273 **3.6 Comment on unitarization issues**

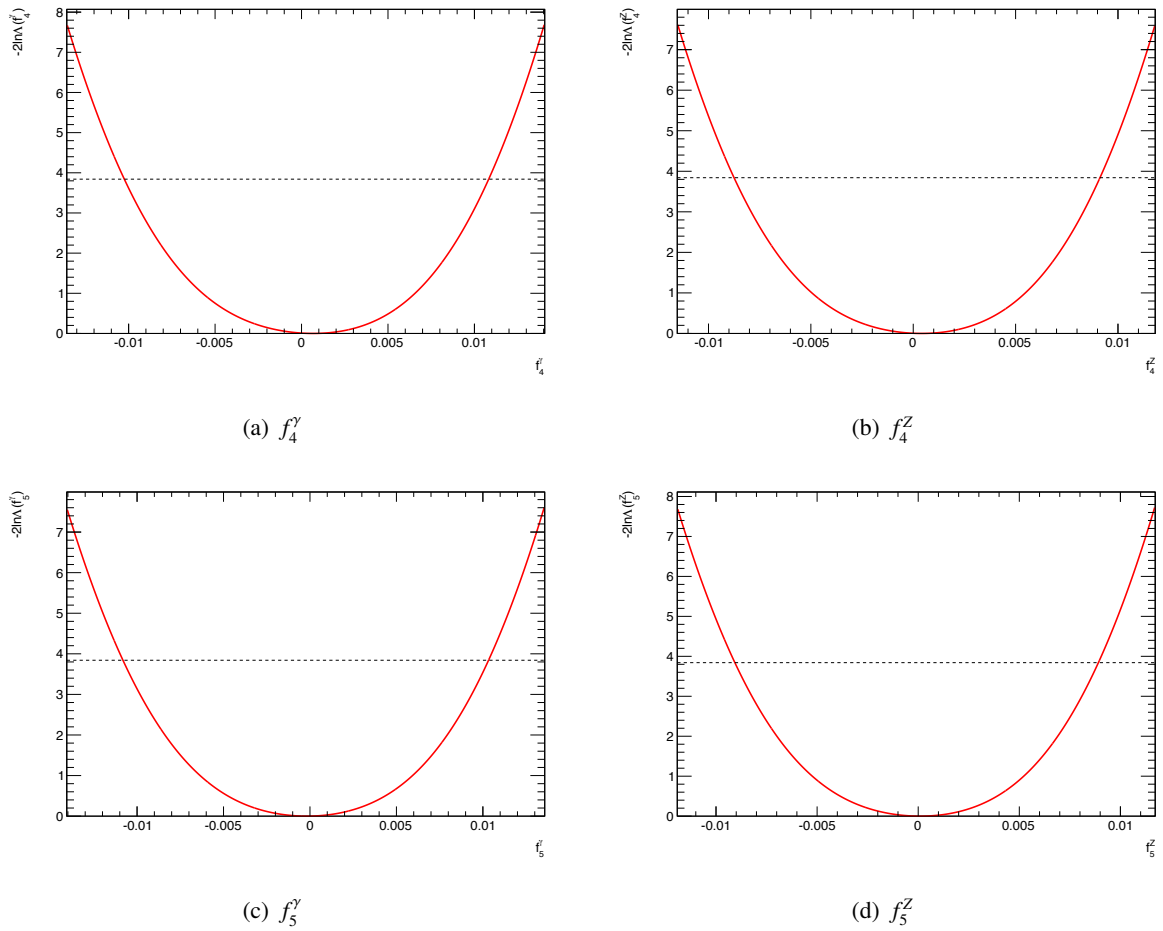


Figure 3: Plots of the test statistic, t_α , as a function of aTGC value made with truncated Gaussian constraints. Dashed line marks the 95% C.I. cutoff values.

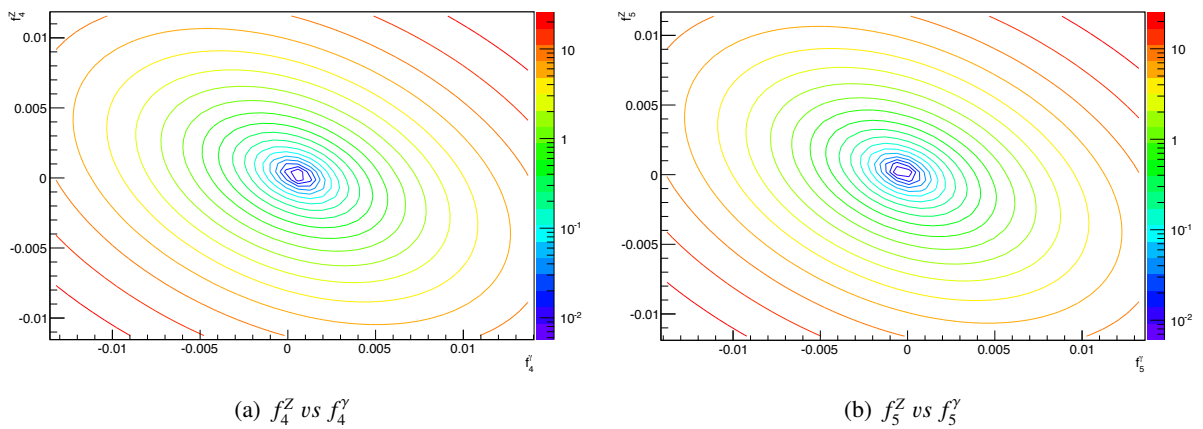


Figure 4: Plots of the test statistic, t_α , as a function of aTGC value made with truncated Gaussian constraints.

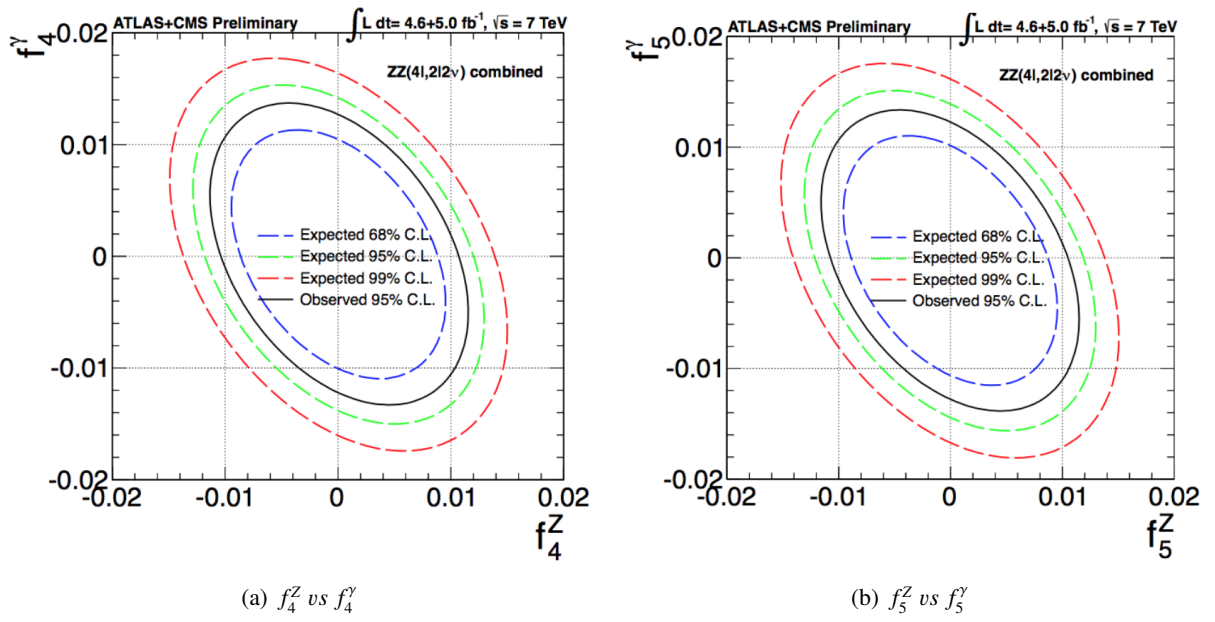


Figure 5: 2D expected and observed ΔNLL combined limits with log-normal constraints.

274 **4 Conclusions**

References

- 275
- 276 [1] ATLAS Collaboration Collaboration, G. Aad et al., *Measurement of ZZ production in pp*
277 *collisions at $\sqrt{s} = 7$ TeV and limits on anomalous ZZZ and ZZ γ couplings with the ATLAS*
278 *detector*, JHEP **1303** (2013) 128, arXiv:1211.6096 [hep-ex].
- 279 [2] M. Cacciari, G. P. Salam, and G. Soyez, *The Anti-k(t) jet clustering algorithm*, JHEP **0804** (2008)
280 063, arXiv:0802.1189 [hep-ph].
- 281 [3] ATLAS Collaboration Collaboration, G. Aad et al., *Measurement of the top quark pair cross*
282 *section with ATLAS in pp collisions at $\sqrt{s} = 7$ TeV using final states with an electron or a muon*
283 *and a hadronically decaying τ lepton*, Phys.Lett. **B717** (2012) 89–108, arXiv:1205.2067
284 [hep-ex].
- 285 [4] CMS Collaboration Collaboration, S. Chatrchyan et al., *Measurement of the ZZ production cross*
286 *section and search for anomalous couplings in 2 l2l' final states in pp collisions at $\sqrt{s} = 7$ TeV*,
287 JHEP **1301** (2013) 063, arXiv:1211.4890 [hep-ex].
- 288 [5] K. Hagiwara et al., *Probing the weak boson sector in $e^+e^- \rightarrow W^+W^-$* , Nucl. Phys. B **282** (1987)
289 253.
- 290 [6] T. G. et al., *Event generation with Sherpa 1.1*, JHEP **0902** (2009) 007, arXiv:0811.4622
291 [hep-ph].
- 292 [7] U. Baur and D. L. Rainwater, *Probing neutral gauge boson self interactions in ZZ production at*
293 *hadron colliders*, Phys. Rev. D **62** (2000) 113011, arXiv:0011016 [hep-ph].
- 294 [8] J. O. U. Baur, T. Han, *WZ production at hadron colliders: Effects of non-standard WWZ couplings*
295 *and QCD corrections*, Phys. Rev. D **51** (1995) 3381, arXiv:9410266 [hep-ph].
- 296 [9] J. O. U. Baur, T. Han, *QCD corrections and anomalous couplings in Z production at hadron*
297 *colliders*, Phys. Rev. D **57** (1998) 2823, arXiv:9710416 [hep-ph].
- 298 [10] R. D. C. Gary J. Feldman, *A Unified Approach to the Classical Statistical Analysis of Small*
299 *Signals*, JHEP Phys.Rev **D57** (1998) 3873, arXiv:9711021 [hep-ex].
- 300 [11] T. Junk, *Confidence level computation for combining searches with small statistics*, Nucl. Instrum.
301 Meth. **A434** (1999) 435, arXiv:9902006 [hep-ex].
- 302 [12] A. Read, *Presentation of search results: the CLs technique*, J. Phys. **G28** (2002) 2693.
- 303 [13] A. collaboration, *Procedure for the LHC Higgs boson search combination in summer 2011*,
304 CERN, Geneva Switzerland (2011).